Switching function parameter variation analysis of a quasi-sliding mode controlled induction motor drive

Shaija Palackappillil[1,2], Asha Elizabeth Daniel[1]
[1]Division of Electrical & Electronics Engineering, School of Engineering, Cochin University of Science and Technology, Kochi, India
[2]Department of Electrical & Electronics Engineering, Government Model Engineering College, Kochi, India

ABSTRACT

Sliding mode control is a nonlinear, robust control that is having better load disturbance rejection capability, less parameter sensitivity and fast dynamic response. Conventional sliding mode control introduces high chattering that can degrade the induction motor (IM) drive system responses. Hence, a quasi-sliding mode controller (Q-SMC) using a hyperbolic tangent function coupled with equivalent control is designed for robust speed control of vector-controlled IM drive in this work. This work focuses on the effect of variation of the switching function parameters of the Q-SMC on the performance of the drive. Extensive simulations are performed using MATLAB/Simulink software, and the switching function parameters are adjusted across a wide range and its impact on motor performance is studied qualitatively and quantitatively, with accompanying graphical results and various transient parameters. It is observed that a Q-SMC controller with a larger boundary layer width has less overshoot, less steady-state error, and a lower current THD. It is also observed that even though a high gain Q-SMC controller responds quickly, the percentage overshoot for high gain systems is likewise large. Hence, if the boundary layer width and switching gain parameters are optimized, a Q-SMC speed controller is a promising choice for a high-performance IM drive.

Corresponding Author:

Shaija Palackappillil
Division of Electrical & Electronics Engineering, School of Engineering
CUSAT, Kochi, Kerala, India
Email: shaijapj@gmail.com

1. INTRODUCTION

Advances in power electronics, microcontrollers, processor-based systems, and nonlinear control theory have facilitated substantial research into advanced control approaches for induction motor (IM) drives during the last few decades. Despite the fact that induction motors are extremely complex, nonlinear, and tightly coupled [1], numerous researchers have developed various strategies for its dynamic control without compromising performance. Model predictive control (MPC) [2], Field oriented control (FOC), direct torque control (DTC) [3], feedback linearization (FL) [4] and observer-based nonlinear controllers [5] have all been presented in the literature to achieve quick dynamic responses in IM. Various sophisticated speed control approaches such as robust control, optimal control, adaptive control [6], sliding mode control (SMC) [7], and intelligent control techniques like fuzzy logic control [8], [9] and artificial neural network (ANN) are also being developed.

In this work, an indirect field-oriented control (IFOC) or indirect vector control (IVC) is applied to the IM drive. There are two control loops in vector control. The inner loop controls current, whereas the outer loop controls speed [10]. Hysteresis controller is used in the inner current loop. Classical fixed gain

proportional-integral (PI) controller based IFOC drives fail to provide the desired performance when load perturbations, parametric variations [11], external disturbances or modelling uncertainties [12] are there, making the torque sluggish and oscillatory [13], which may become critical in certain applications. To address this application-oriented challenge a sliding mode controller is proposed as the speed controller in this work.

Sliding mode control is a type of nonlinear control that has two design modes: i) sliding surface design and ii) sliding mode controller design. The sliding surface has to ensure the desired transient and steady-state behaviours in it, while the controller has to accelerate the system trajectory to reach the sliding surface asymptotically or in finite time [14], [15] and to remain there afterwards, eventually attaining exact tracking asymptotically or in finite time [16]. Conventional SMC utilizes a simple sign function for switching, resulting in high-frequency chattering in the control output [17]. Control of the direct current regulated IM drive is done using conventional SMC and boundary SMC using a saturation function in [18]. Nguyen *et al.* [19] discusses the sliding mode control of a stator-flux-oriented three-phase IM. SMC with a fuzzy mutual reference adaptive system observer is used to estimate the speed of an IM drive in [20].

A quasi-sliding mode controller (Q-SMC) with a smooth hyperbolic tangent function is proposed in this work as the speed controller in order to reduce the chattering issue of conventional SMC and is applied in an indirect rotor field-oriented control (IRFOC) scheme. As the parameters of the switching function are varied, the performance of the induction motor will be affected. This work focus to investigate on the effect of variation of these switching function parameters on the performance of the drive. The major contributions of this work include the design of indirect rotor field-oriented control scheme of IM drive, design of a chatter-free quasi-sliding mode control using a hyperbolic tangent function coupled with equivalent control, performance comparison of Q-SMC with conventional SMC and qualitative and quantitative analysis of the impact of Q-SMC switching function parameter variation on motor performance.

This paper is organized as: section 2 presents the mathematical formulation of the sliding mode control system in the IFOC induction motor drive system. Section 3 introduces the design of the Q-SMC with a hyperbolic tangent switching function. The results and discussion are given in section 4 and the conclusion in section 5.

2.   SLIDING MODE SPEED CONTROL IN IFOC INDUCTION MOTOR DRIVE

The sliding mode speed control approach for vector-controlled induction motors is covered in this section. Here, the rotor flux angle is obtained indirectly from the slip angle speed ω_{sl}. A sliding mode controller is used as the speed controller.

2.1. IFOC induction motor drive

The block diagram of the induction motor drive based on the indirect vector control strategy is shown in Figure 1. Decoupling between the motor flux and torque is obtained by choosing a synchronously rotating reference frame to model the induction motor and by aligning it in the direction of rotor flux. A hysteresis current controller is employed to generate gate pulses to the 2-level inverter. The currents i_{qs} and i_{ds} are found from the *d-q* transformation of sensed stator currents i_a, i_b and i_c using clarke's and park's transformations. The q-axis component of current i_{qs} is responsible for the production of torque and the d-axis component i_{ds} for the flux. Rotor speed is measured by the encoder and these inputs are used to estimate the rotor flux (φ_r) and slip speed (ω_{sl}) in a feed-forward manner [9]. Flux rotor position (θ_e) obtained is necessary for d-q to a-b-c and a-b-c to d-q transformations. The actual speed measured is compared with the command speed and speed error is used for generating the sliding surface in SMC and the SMC output is the reference torque component of current (i_{qs}^*). The reference flux component of current (i_{ds}^*) deduced from the desired rotor flux is keyed into the controller. Reference i_{ds}^* and i_{qs}^* are converted to i_a^*, i_b^* and i_c^* and the hysteresis current controller generates the switching pulses according to the sensed stator current i_a, i_b and i_c [21]. The power circuit consists of a DC supply and a two-level IGBT inverter feeding the three-phase induction motor.

The developed torque is given by [8], [9], [13].

$$T_e = \frac{3}{2} \cdot \frac{P}{2} \cdot \frac{L_m}{L_r} \left(i_{qs} \cdot \psi_{dr} - i_{ds} \cdot \Psi_{qr} \right) = \frac{3}{2} \cdot \frac{P}{2} \cdot \frac{L_m}{L_r} \left(i_{qs} \cdot \psi_{dr} \right) \tag{1}$$

As $\psi_{qr} = 0$, in rotor field oriented control [22]. Here, *P* represents the number of poles, L_m represents magnetizing inductance, L_r represents the self-inductance of the rotor, ψ_{dr} and ψ_{qr} represent rotor d-q-axes flux linkages.

$$T_e = K_T i_{qs} \tag{2}$$

Where

$$K_T = \frac{3}{2} \cdot \frac{P}{2} \cdot \frac{L_m}{L_r} \psi_{dr} * \tag{3}$$

$\psi_{dr} *$ is the command rotor flux.

The governing equation of the motor shaft and the load dynamics is given by [16],

$$T_e - T_L = J \frac{d\omega_m}{dt} + B \cdot \omega_m \tag{4}$$

where J represents inertia (kg-m^2) and ω_m mechanical speed of the rotor (rad/s). T_e, T_L represents electromagnetic and mechanical or load torque (N.m.) while B represents the frictional coefficient (Nm.S). Using (2) and (4), the speed dynamics state-space model is obtained as,

$$\frac{d\omega_m}{dt} = \frac{K_T}{J} i_{qs} - \frac{B}{J} \omega_m - \frac{T_L}{J} \tag{5}$$

using state variables $x_1 = \omega_m$, $x_2 = \dot{x}_1$ and control input $u = i_{qs}$, the dynamic speed equation can be stated as,

$$\dot{x}_1 = -\frac{B}{J} x_1 + \frac{K_T}{J} u - \frac{T_L}{J} \tag{6}$$

$$\dot{\omega}_m (t) = a \omega_m + b i_{qs} * + d T_L \tag{7}$$

where, $a = -\frac{B}{J} < 0$, $b = \frac{K_T}{J} > 0$ and $d = -1/J < 0$

Figure 1. Indirect vector controlled IM with sliding mode speed controller

2.2. Sliding mode control

Using the equivalent control approach, a sliding mode control system can be written in general as [22],

$$\dot{x} = f(x) + g(x).u_c \text{ and } y = h(x) \tag{8}$$

Where $u_c(t)$ is the control signal input and $y(t)$ is the system output. As per the equivalent control technique, the control signal $u_c(t)$ can be stated as [23],

$$u_c = u_{eq} + u_{sc} \tag{9}$$

Where u_{eq} is the equivalent control action in charge of ensuring system convergence and u_{sc} is the switching control action in charge of ensuring that the sliding surface is drawn to the system state space. The controller task is to make the motor run at a speed ω_m that correctly track the command speed ω_{ref} even in the occurrence of model imperfections, load torque disturbances and measurement noise.

2.2.1. Equivalent control

Taking into account the parametric fluctuations, external disturbances and uncertainties, as well as the unmodeled dynamics for the actual induction motor drive, dynamic in (7) can be rewritten as [13]:

$$\dot{\omega}_m = (a + \Delta a)\omega_m + (b + \Delta b)\, i_{qs} * + (\text{d} + \Delta d)\, T_L \tag{10}$$

$$\dot{\omega}_m\,(t) = a\,\omega_{m(t)} + b\, i_{qs} * + L(t) \tag{11}$$

Where L(t) represents the lumped uncertainty parameter [24], and it can be written as,

$$L\,(t) = (\Delta a)\omega_{m(t)} + (\Delta b)\, i_{qs} * + (\text{d} + \Delta d)T_L \tag{12}$$

and the terms Δa, Δb and Δd represent the uncertainties associated with the respective terms [25]. The speed error can be stated as (13):

$$e(t) = \omega_{ref(t)} - \omega_{m(t)} \tag{13}$$

where, $\omega_{ref(t)}$ is the speed reference and $\omega_{m(t)}$ is the actual rotor speed. From (11) and (13),

$$\dot{e}(t) = \dot{\omega}_{ref(t)} - a\,\omega_{m(t)} - b\, i_{qs} * - L(t) \tag{14}$$

$$i_{qs} * = \frac{1}{b}[\,\dot{\omega}_{ref(t)} - a\,\omega_{m(t)} - L(t) - \dot{e}(t)] \tag{15}$$

2.2.2. Sliding surface

The sliding plane S is designed as a function of the speed error $e(t)$, its integral $\int e.dt$, and its derivative $\dot{e}(t)$ and can be written as (16).

$$S = \dot{e} + \lambda_1 e + \lambda_2 \int e\, dt \tag{16}$$

Where λ_1 and λ_2 are positive real surface parameters and these gain parameters define the slope of the sliding manifold. The convergence of this set of equations can be demonstrated using the lyapunov energy function V [23], [26].

$$V = \frac{1}{2}S^2 \tag{17}$$

2.2.3. Switching function and switching control

In conventional SMC, the switching function used is the sign function which is defined as [27] (18).

$$sgn(S) = \begin{cases} +1, & if\, s > 0 \\ -1, & if\, s < 0 \end{cases} \tag{18}$$

The switching control component is given by [5],

$$u_{sc} = \beta_c sgn(S) \tag{19}$$

where β_c is the sliding coefficient.

As the uncertainty bound is difficult to estimate in practice, this coefficient must be set to a large enough value so as to overcome the effect of any external disturbance [27]. This conventional SMC is very simple, but it causes high chattering because of the discontinuous nature of its switching function. Chattering is highly undesirable as it causes excessive control activity, increased power consumption and increased torque ripples [26] and thereby causes the deterioration of overall system performance in IM drives. Hence in this work, a quasi sliding mode control (Q-SMC) using a continuous hyperbolic tangent (tanh) function [28], [29] is used which is discussed in section 3.

3. QUASI-SLIDING MODE SPEED CONTROL

To deal with the high-frequency chattering issue, quasi-sliding mode controller (Q-SMC) is proposed that will make the state stay in a certain range at boundary layer neighborhood. Specifically, a continuous hyperbolic tangent (tanh) function is proposed in this work instead of the discontinuous signum function. Even with nonlinear control input, the chaos linked with a motor subjected to unmatched

uncertainty can be effectively suppressed or driven to a predictable and controlled bound using a quasi-sliding mode control (Q-SMC) approach.

3.1. Switching function

The hyperbolic tangent function is given by (20) and is shown in Figure 2.

$$tanh\left(\frac{s}{\epsilon}\right) = \frac{e^{\left(\frac{s}{\epsilon}\right)} - e^{-\left(\frac{s}{\epsilon}\right)}}{e^{\left(\frac{s}{\epsilon}\right)} + e^{-\left(\frac{s}{\epsilon}\right)}} \qquad (20)$$

Where ε is the boundary layer width and it determines the steepness or inclination of the tanh function (ε>0). As the value of ε is close to zero, the switching function will approximate the sign function. The switching control component is given by,

$$u_{sc} = \zeta_M \ tanh\left(\frac{s}{\epsilon}\right) \qquad (21)$$

The switching gain ζ_M is the output saturation value of the controller. Switching gain is employed in sliding mode as the upper bound of uncertainties. The hyperbolic tangent function is a good choice for the noisy IM control system as it is having a smoother behaviour near saturation.
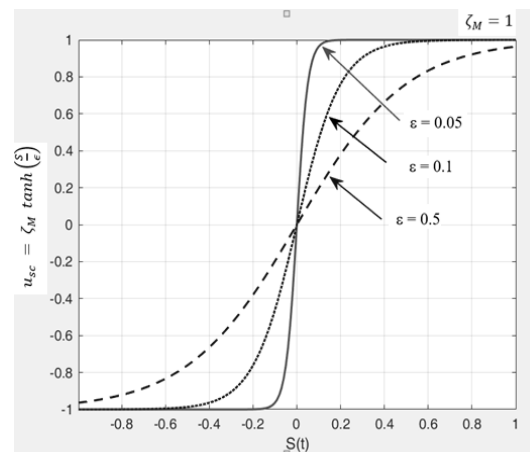
Figure 2. Tanh function as switching function in Q-SMC

3.2. Switching function parameters

The two parameters of the adopted hyperbolic tangent switching function are the switching gain ζ_M and the boundary layer width ε. The effect of variation of these two parameters on the performance of the IM drive is investigated in Section 4. The transient parameters are also analyzed and discussed in the next section.

4. RESULTS AND DISCUSSION

The quasi-sliding mode speed controller based on tanh function discussed in the previous section is developed in MATLAB/ Simulink software for a 10HP IFOC induction motor drive and the effect of variation of the switching parameters ζ_M and ε on the performance of the motor are investigated separately in this section. The hysteresis band h taken is 0.05. The nominal value of flux, φ_{ref} is taken as 0.8 pu. Table 1 shows the specifications of the squirrel cage induction motor under investigation.

Table 1. Induction motor parameters

Parameter	Value	Parameter	Value
Power	7500 W	Nominal torque	49 Nm
Rs	0.7384 Ω	J	0.0943 kg m2
Rr	0.7402 Ω	B	0.000503kg m2/s
Ls	127.1 e−3H	Pole pairs	2
Lr	127.1e−3H	Speed (rated)	1440 rpm
Lm	124.1e−3H	Voltage (rated)	400V, 3φ

4.1. Comparison between conventional SMC and Q-SMC

Figure 3 depicts the speed response of a traditional SMC controller with a sign switching function and a Q-SMC controller with a tanh switching function when subjected to a reference speed of 1440 rpm. It is observed from the graph that the conventional SMC produces a lot of chattering whereas the oscillations in the Q-SMC speed response die out very quickly. Also, the percentage of overshoot and undershoot are high in conventional SMC compared to Q-SMC.
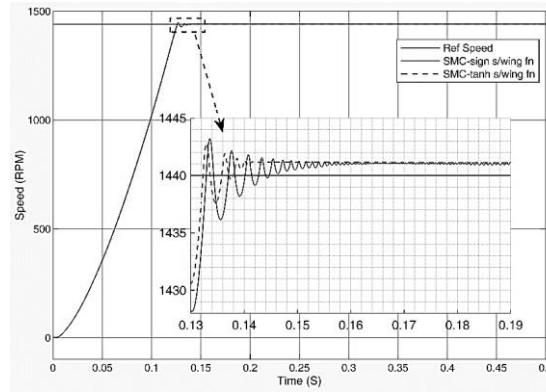
Figure 3. Speed response of conventional SMC and Q-SMC

4.2. Case 1: Variation in epsilon (ϵ) parameter of Q-SMC
4.2.1. Under no load and a command speed of 1440RPM

In this investigation, a command speed of 1440RPM is applied to the indirect vector-controlled IM drive under no-load condition and is simulated for 1.0S duration. The switching gain ζ_M is set as 100. The simulation study is carried out with epsilon (ϵ) values of 0.1, 1 and 10 and corresponding graphs are plotted below. The zoomed-in view of transient speed response from 0.12S to 0.18S with the three epsilon values is shown in Figure 4. It is evident from the graph that the Q-SMC with lower epsilon (ϵ) value is having greater overshoot and high chattering.

The steady-state current graph corresponding to epsilon (ϵ) values 0.1, 1 and 10 from 0.9S to 1S are shown in Figure 5. The switching gain ζ_M is maintained as 100 itself. Corresponding torque responses are plotted in Figure 6. The chattering is high for epsilon (ϵ) value 0.1 as observed from Figure 5 and Figure 6.
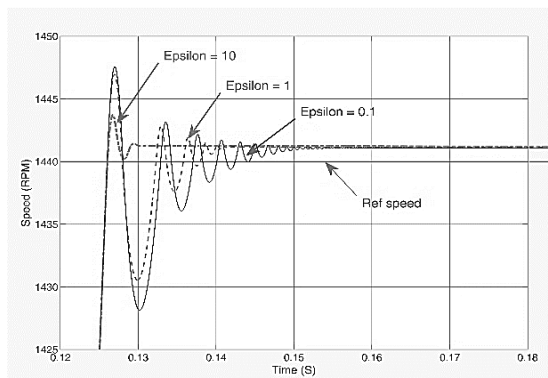
Figure 4. Speed responses for different ϵ values
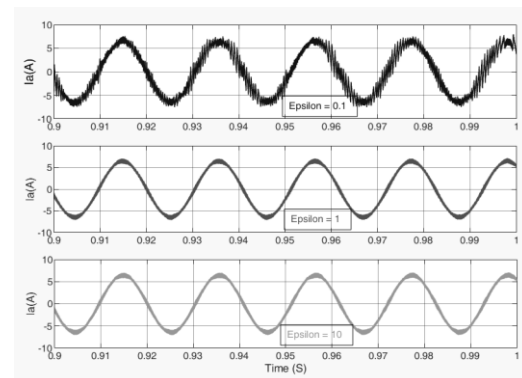
Figure 5. Stator current I_a for different ϵ values

4.2.2. Under full load and a command speed of 1440RPM

The simulation experiment is repeated for Full load torque at a command speed of 1440RPM and with ζ_M 100. The corresponding speed responses are shown in Figure 7. The stator current I_a for different epsilon (ϵ) values are shown in Figure 8 and the torque responses in Figure 9. Here, all the three response graphs reveal that the Q-SMC with lower epsilon (ϵ) value is having greater overshoot and high chattering

under loaded conditions also. The sliding surface S for $\zeta_M =100$ and for different epsilon (ε) values are shown in Figure 10. The zoomed-in view is shown as a subplot in Figure 10 for a better understanding. The figure shows that the sliding surface follows the same path and very quickly reaches zero and afterwards maintain the state due to the controller action in all three cases. For a higher value of epsilon (ε), the sliding surface is not confining to exactly zero.
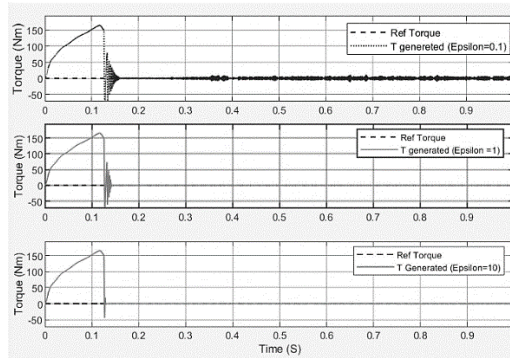

Figure 6. Torque responses for different epsilon (ε) values
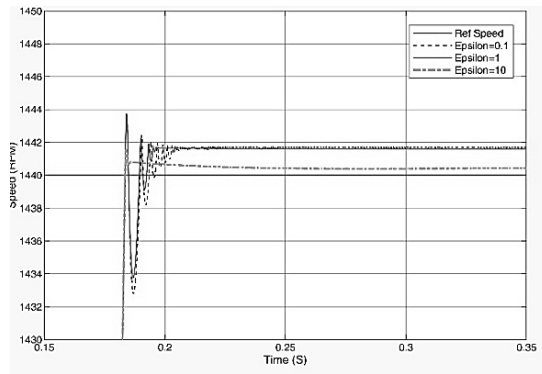
Figure 7. Speed responses under full load for different epsilon (ε) values
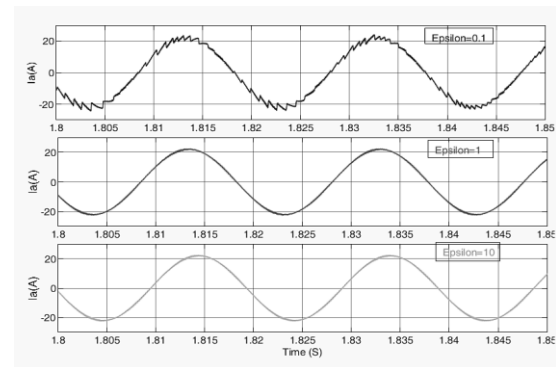
Figure 8. Stator Current I_a under full load for different epsilon (ε) values
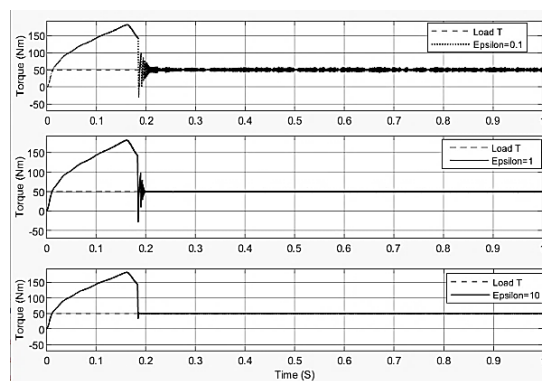
Figure 9. Torque responses under full load for different epsilon (ε) values
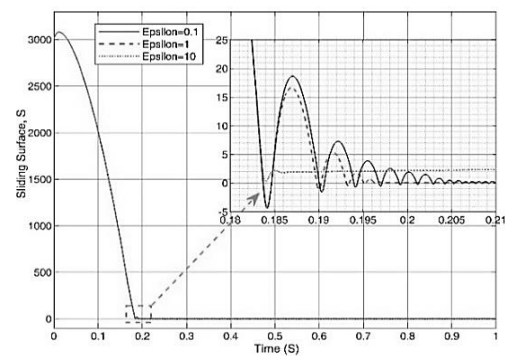
Figure 10. Sliding surface S for different epsilon (ε) values

4.2.3. Transient performance analysis

The transient performance analysis with the different epsilon (ε) values are carried out in simulation for Q-SMC for a command speed of 1440RPM and for no-load and full load condition and is recorded in Table 2. It can be found that the controller with lower epsilon (ε) value gives higher overshoot, higher steady-

state error and high current THD under no-load and loaded cases. The change in epsilon (ε) values do not affect the rise time or settling time as observed from Table 2. It can be concluded that the larger the width of the boundary layer, the smoother the control signal [30]. Even though the boundary layer design is intended to reduce chattering, it does not drive the system state to the origin but instead has a small residual set around the origin. That is, a wide boundary layer width is preferable for control signal smoothness, whereas a small boundary layer width is chosen for control accuracy. Hence an optimum value of boundary layer width should be selected for better performance.

Table 2. Transient parameters and current THD when epsilon (ε) is varied

Transient Parameters	For N=1440 RPM, No Load, ξ_m=100			For N=1440 RPM, Full Load, ξ_m=100		
	$\varepsilon = 0.1$	$\varepsilon = 1$	$\varepsilon = 10$	$\varepsilon = 0.1$	$\varepsilon = 1$	$\varepsilon = 10$
Rise Time (S)	0.0886	0.0886	0.0886	0.1125	0.1125	0.1124
Settling Time (S)	0.1242	0.1242	0.1242	0.1806	0.1806	0.1806
Peak Time (S)	0.127	0.1269	0.1267	0.1842	0.1842	0.184
Peak Value(RPM)	1447.6	1447	1443.7	1443.8	1443.7	1441.6
Overshoot (%)	0.53	0.49	0.26	0.26	0.26	0.11
S S Error (%)	0.08	0.08	0.07	0.12	0.11	0.05
Current THD (%)	19.59	7.65	6.05	5.53	2.71	2.31

4.3. Case 2: Variation in switching gain (ζ_M)of Q-SMC
4.3.1. Under no load and a command speed of 1/3rd rated speed (480RPM) with epsilon (ε) = 1

In this study, a command speed of 1/3rd rated speed (480RPM) is applied to the IM drive under the no-load condition with boundary layer width ε set as 1 and is simulated for 1.0S duration. The simulation work is carried out with a switching gain ζ_M of 50, 100 and 150 respectively. Corresponding graphs are plotted with all the three ζ_M values. Figure 11 shows the reference speed and actual speed response obtained with the three switching gain values. The zoomed-in view of transient speed response from 0.04S to 0.14S is given as a subplot in it. It can be observed from the plot that, as the gain (ζ_M) is reduced, predominant oscillations in the speed graph are reduced and response becomes slower. The controller with ζ_M value 50 took a much higher time to reach its peak than the system with ζ_M value 150. Also, the higher the gain, the greater the percentage overshoot. The corresponding stator current graphs are shown in Figure 12 and the torque responses in Figure 13.
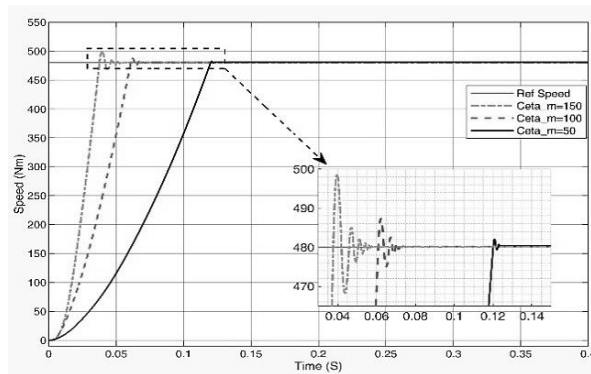

Figure 11. Speed responses for different gain (ζ_M) values
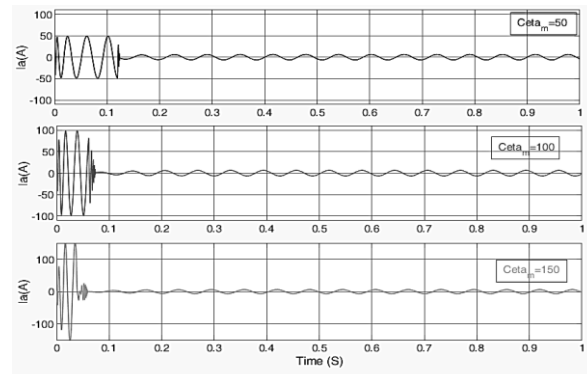

Figure 12. Stator current I$_a$ for different gain (ζ_M) values

4.3.2. Under half load and a command speed of 1/3rd rated speed (480RPM) with epsilon (ε) = 1

The simulation experiment is repeated for half load torque at a command speed of 480RPM and with ε of 1. The corresponding speed responses for different gain (ζ_M) values are shown in Figure 14 and its enlarged view as a subplot in it. The Torque responses for different gain (ζ_M) values are shown in Figure 15. Here, all the three response graphs reveal that the Q-SMC with higher Gain (ζ_M) is having a fast dynamic response, large overshoot and high oscillations under loaded conditions also. The sliding surface s for ε=1 and for different gain (ζ_M) values are plotted in Figure 16. It shows that the sliding surface S takes different paths to reach the sliding manifold S=0 as the gain parameter ζ_M is varied and afterwards maintain the state due to the controller action in all the three cases with different gain (ζ_M) values.
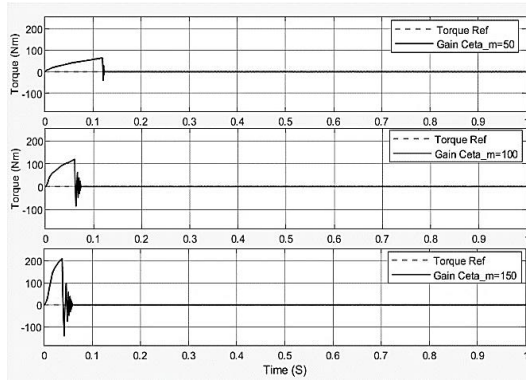
Figure 13. Torque responses under no load for different switching gain (ζ_M) values
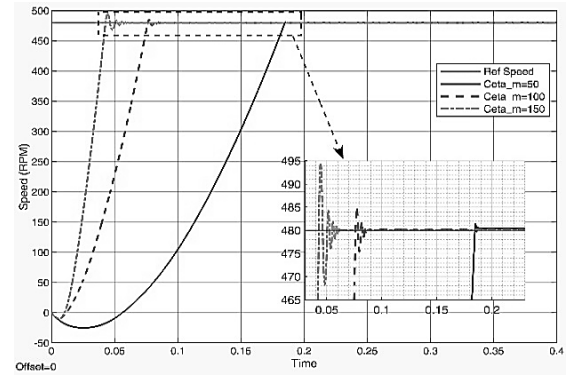

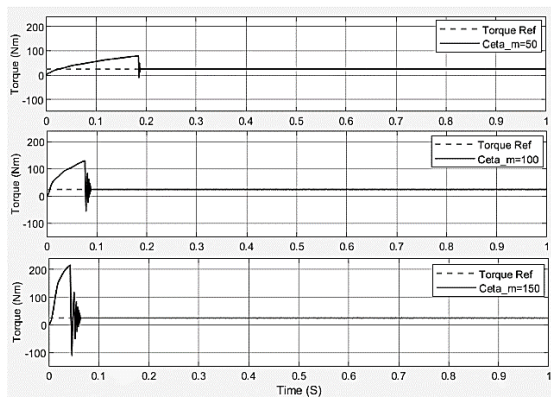Figure 14. Speed responses under half load for different switching gain (ζ_M) values

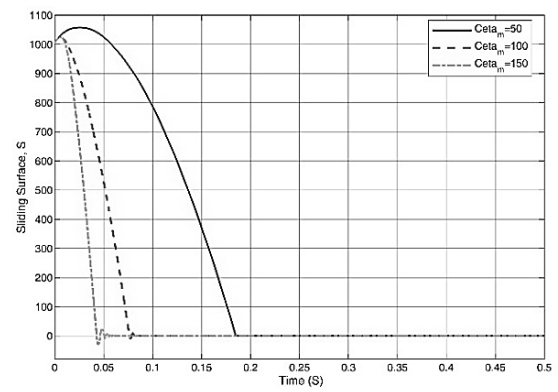Figure 15. Torque responses under half load for different switching gain (ζ_M) values

Figure 16. Sliding surface S for different switching gain (ζ_M) values

4.3.3. Transient performance analysis

The transient performance analysis with the different switching gain (ζ_M) values are carried out in simulation for Q-SMC for a command speed of 480RPM and a load torque of 0 Nm (No Load) and 24.75 Nm (Half Load) and is recorded in Table 3. By analysing the Table data, we can conclude that rise time, settling time, peak time and steady-state error are higher for systems with lower gain (ζ_M) values under no-load and loaded conditions. That means the Q-SMC with higher switching gain responds quickly. Even though the dynamic response of high gain systems is fast, the percentage overshoot is also high for high gain systems and it is to be limited in IM drive applications. The current THD value is more or less the same in all systems with different switching gain (ζ_M) values as compared to case 1.

So, it can be concluded that the magnitude of chattering is proportional to switching gain which represents the upper bound of uncertainties of the system. If this upper bound selected is too large, the switching control law will result in a serious chattering phenomenon. Contrarily, if the bound selected is too small, the stability conditions may not be met. Hence, an adequate switching gain value should be chosen to decrease the amplitude of chattering at the same time preserving the existence of sliding mode control.

Table 3. Transient parameters and current THD when switching gain (ζ_M) is varied

Transient Parameters	For N=1/3rd speed=480RPM, No Load, ε =1			For N=1/3rd speed=480RPM, Half Load, ε =1		
	ξ_m =50	ξ_m =100	ξ_m =150	ξ_m =50	ξ_m =100	ξ_m =150
Rise Time (S)	0.0833	0.0417	0.0224	0.0962	0.0478	0.024
Settling Time (S)	0.1186	0.0601	0.0446	0.183	0.0754	0.0491
Peak Time (S)	0.1208	0.0622	0.0396	0.1853	0.0773	0.0445
Peak Value (RPM)	482.16	487.4	498.7	481.44	485.1	494.44
Overshoot (%)	0.45	1.54	3.90	0.30	1.06	3.01
S S Error (%)	0.07	0.04	0.03	0.11	0.04	0.02
Current THD (%)	3.12	3.08	3.05	2.06	1.96	1.82

5.   CONCLUSION

In this paper, the design of a quasi-sliding mode speed controller for the IM drive is presented with hysteresis current controller. The indirect vector control technique and the quasi- sliding mode speed controller as applied to an induction motor drive is discussed. The signum switching function of conventional SMC is replaced by the hyperbolic tangent function to make it a smooth function instead of a discontinuous function. In this work, the boundary layer width ε and the switching gain ζ_M of the tanh function are varied across a range of 0.01 to 10 and 50 to 150 respectively and its effect on the IM drive performance is investigated both qualitatively and quantitatively. Extensive simulations are carried out with applied switching function parameter variations and the resulting impacts on the drive performance are analysed graphically. Transient analysis parameters and current THD are also tabulated that represent a quantitative measure of the effect of variation of switching function parameters on drive performance. A boundary layer width that is too small results in significant overshoot and chattering. Choice of boundary layer width is a trade-off between smoothness of the control signal and control accuracy. High value of switching gain results in high overshoot and chattering in spite of a fast stabilized system response. Hence a Q-SMC with an optimum value of boundary layer width and switching gain parameter results in enhanced performance of the IM drive.

REFERENCES

[1]   R Krishnan, "Vector-controlled Induction Motor drives," *Modern Power Electronics and AC Drives*, PHI Publications, 2009.
[2]   F. Wang, Z. Zhang, X. Mei, J. Rodríguez and R. Kennel, "Advanced Control Strategies of Induction Machine: Field Oriented Control, Direct Torque Control and Model Predictive Control," *Energies*, vol. 11,no. 1, pp. 1-13, 2018; doi:10.3390/en11010120.
[3]   S. Hussain and M. A. Bazaz, "Review of vector control strategies for three phase induction motor drive," *International Conference on Recent Developments in Control, Automation and Power Engineering (RDCAPE)*, 2015, pp. 96-101, doi: 10.1109/RDCAPE.2015.7281376.
[4]   A. Devanshu, M. Singh and N. Kumar, "Sliding Mode Control of Induction Motor Drive Based on Feedback Linearization," *IETE Journal of Research*, vol. 66, no. 2, pp. 256-269, 2020, doi: 10.1080/03772063.2018.1486743.
[5]   R. Gunabalan and V. Subbiah, "Implementation of Field Oriented Speed Sensor less Control of Induction Motor Drive," *International Journal on Electrical Engineering and Informatics*, vol. 8, no. 4, pp. 727-738, 2016, doi: 10.15676/ijeei.2016.8.4.2.
[6]   M. Madark, A. B. Razzouk, E. Abdelmounim, and M. E. Malah, "A New Induction Motor Adaptive Robust Vector Control based on Backstepping," *International Journal of Electrical and Computer Engineering*, vol. 7, no. 4, pp. 1983-1993, 2017; doi: 10.11591/ijece.v7i4.pp1983-1993.
[7]   M. Aktas, K. Awaili, M. Ehsani, and A. Arisoy, "Direct torque control versus indirect field-oriented control of induction motors for electric vehicle applications," *Engineering Science and Technology, an International Journal,* vol. 23, no. 5, pp. 1134-1143, 2020, doi:10.1016/j.jestch.2020.04.002.
[8]   P. J. Shaija P J and Asha Elizabeth Daniel, "An Intelligent Speed Controller Design for Indirect Vector Controlled Induction Motor Drive System," *Procedia Technology,* vol. 25, pp 801-807, 2016. doi: 10.1016/j.protcy.2016.08.177.
[9]   K. Zeb, Z. Ali, K. Saleem, W. Uddin, M. A. Javed, and N. Christofides, "Indirect field-oriented control of induction motor drive based on adaptive fuzzy logic controller," *Electrical Engineering (Springer),* vol. 99, pp. 803-815, 2016, doi:10.1007/s00202-016-0447-5.
[10] V. T. Ha, T. T. Minh, N. T. Lam, and N. H. Quang, "Experiment based comparative analysis of stator current controllers using predictive current control and proportional integral control for induction motors," *Bulletin of Electrical Engineering and Informatics,* vol. 9, no. 4, pp. 1662-1669, 2020, doi: 10.11591/eei.v9i4.2084.
[11] A. Ghezouani, B. Gasbaoui and J. Ghouili, "Sliding Mode Observer-based MRAS for Sliding Mode DTC of Induction Motor: Electric Vehicle," *International Journal on Electrical Engineering and Informatics*, vol. 11, no. 3, pp. 580-595, 2019, doi: 10.15676/ijeei.2019.11.3.9.
[12] G. Tarchała and T. O. Kowalska, "Discrete Sliding Mode Speed Control of Induction Motor Using Time-Varying Switching Line," *Electronics, MDPI*, vol. 9, no1, pp. 1-18, 2020, doi:10.3390/electronics9010185.
[13] H. A. Maksoud, T. Fetouh, M. S. Zaky and H. Z.. Azazi, "High suppression of disturbances and parameters mismatch for IM drives using a novel VSC," *Journal of Electrical Systems*, vol. 14, no. 4, pp. 48-63, 2018.
[14] A. Mousmi, A. Abbou, Y. El. Houm, and A. Bakouri, "Real time implementation of a super twisting control of a BLDC motor," *International Journal of Electrical and Computer Engineering (IJECE),* vol. 9, no. 4, pp. 3032-3040, 2019, doi: 10.11591/ijece.v9i4.pp3032-3040.
[15] F. Xu, N. An, J. Mao and S. Yang, "A New Variable Exponential Power Reaching Law of Complementary Terminal Sliding Mode Control," *Complexity Hindawi*, vol. 20, no. 8874813, pp. 1-11, 2020, doi:10.1155/2020/8874813.
[16] O. Barambones and P. Alkorta, "A robust vector control for induction motor drives with an adaptive sliding-mode control law," *Journal of the Franklin Institute,* vol. 348, no. 2, pp. 300–314, 2011, doi:10.1016/j.jfranklin.2010.11.008.
[17] F. R. Yaseen and W. H. Nasser, "Speed Controller of Three Phase Induction Motor Using Sliding Mode Controller," *Iraqi Journal of Computers, Communications, Control & Systems Engineering,* vol. 19, no. 1, pp 52-62, 2019, doi: 10.31026/j.eng.2019.07.07.
[18] A. W. Aditya, M. R. Rusli, B. Praharsena, E. Purwanto, D. C. Happyanto and B. Sumantri, "The Performance of FOSMC and Boundary - SMC in Speed Controller and Current Regulator for IFOC-Based Induction Motor Drive," *International Seminar on Application for Technology of Information and Communication*, 2018, pp. 139-144, doi: 10.1109/ISEMANTIC.2018.8549842.
[19] V. Q. Nguyen, Q. T. Tran and H. N. Duong, "Stator flux-oriented control of three-phase Induction Motors using sliding mode control," *Journal of Electrical Systems*, vol. 16, no. 2, pp. 171-184, 2020.
[20] M. Touam, M. Chenafa, S. Chekroun and R. Salim, "Sensorless nonlinear sliding mode control of the induction machine at very low speed using FM-MRAS observer," *International Journal of Power Electronics and Drive Systems*, vol. 12, no. 4, pp. 1987-1998, 2021, doi: 10.11591/ijpeds.v12.i4.pp1987-1998.

[21] I. C. Ogbuka *et al*, "A robust high-speed sliding mode control of permanent magnet synchronous motor based on simplified hysteresis current comparison," *International Journal of Power Electronics and Drive System,* vol. 12, no. 1, pp. 1-9, 2021; doi: 10.11591/ijpeds.v12.i1.pp1-9.

[22] C. M. R. Oliveira , M. L. Aguiar, J. R. B. A. Monteiro, W. C. A. Pereira, G. T. Paula and T. E. P. Almeida, "Vector Control of Induction Motor Using an Integral Sliding Mode Controller with Anti-windup," *Journal of Control, Automation and Electrical Systems,* vol. 27, no. 2, pp. 169-178, 2016, doi: 10.1007/s40313-016-0228-4.

[23] D. C. Happyanto, A. W. Aditya and B. Sumantri, "Boundary–Layer Effect in Robust Sliding Mode Control for Indirect Field Oriented Control of 3-Phase Induction Motor," *International Journal on Electrical Engineering and Informatics*, vol. 12, no. 2, pp. 188-204, 2020, doi: 10.15676/ijeei.2020.12.2.2.

[24] A. Saghafinia, H. W. Ping, M. N. Uddin and K. S. Gaeid, "Adaptive Fuzzy Sliding-Mode Control Into Chattering-Free IM Drive," *IEEE Transactions on Industry Applications*, vol. 51, no. 1, pp. 692-701, 2015, doi: 10.1109/TIA.2014.2328711.

[25] X. Wang, M. Reitz and E. E. Yaz, "Field Oriented Sliding Mode Control of Surface-Mounted Permanent Magnet AC Motors: Theory and Applications to Electrified Vehicles," *IEEE Transactions on Vehicular Technology*, vol. 67, no. 11, pp. 10343-10356, 2018, doi: 10.1109/TVT.2018.2865905.

[26] F. M. Zaihidee, S. Mekhilef and M. Mubin, "Robust Speed Control of PMSM Using Sliding Mode Control (SMC)—A Review," *Energies,* vol. 12, no. 9, pp. 1-27, 2019; doi:10.3390/en12091669.

[27] S. Massoum, A. Meroufel, A. Massoum and W. Patrice, "DTC based on SVM for induction motor sensorless drive with fuzzy sliding mode speed controller," *International Journal of Electrical and Computer Engineering (IJECE),* vol. 11, no. 1, pp. 171-181, 2021, doi: 10.11591/ijece.v11i1.pp171-181.

[28] S. P Jacob and A. E. Daniel, "Robust Sliding Mode Control Strategy Applied to IFOC Induction Motor Drive," *Fourth International Conference on Electrical, Computer and Communication Technologies (ICECCT)*, 2021, pp. 1-6, doi: 10.1109/ICECCT52121.2021.9616948.

[29] J. S. Fang, J. S. H. Tsai, J. J. Yan and S. M. Guo, "Adaptive Chattering-Free Sliding Mode Control of Chaotic Systems with Unknown Input Nonlinearity via Smooth Hyperbolic Tangent Function," *Hindawi, Mathematical Problems in Engineering,* no. 4509674, pp. pp. 1-10, 2019; doi:10.1155/2019/4509674.

[30] M. Sulaiman, F. A. Patakor and Z. Ibrahim, "A New State-dependent of Sliding Mode Control for Three-Phase Induction Motor Drives," *International Review on Modelling and Simulations*, vol. 6, no. 3, pp. 1-8, 2013.

BIOGRAPHIES OF AUTHORS

Shaija Palackappillil Jacob [iD] [g] [SC] [P] received her B.Tech in Electrical & Electronics Engineering from Mahatma Gandhi University, Kerala, India in 1996 and M.Tech degree in Opto Electronics & Laser Technology from International School of Photonics, Cochin University of Science And Technology (CUSAT), Kerala, India in 2007. She is currently pursuing her PhD in the Division of Electrical Engineering, School of Engineering, CUSAT. She is working as Assistant Professor in the Department of Electrical & Electronics Engineering, Govt. Model Engineering College, Kochi, India. Her research interests include the field of Power Electronics, Motor Drives and Intelligent Control. She can be contacted at email: shaijapj@gmail.com.

Asha Elizebeth Daniel [iD] [g] [SC] [P] is a faculty in the Division of Electrical Engineering at Cochin University of Science and Technology, Kerala, India. She has obtained her B. Tech Degree in Electrical Engineering from NIT Calicut in 1986 and has received her master's and doctoral degrees from IIT Mumbai in 1995 and 2006 respectively. She is currently the Academic Committee Nodal Officer for TEQIP III and the NBA coordinator of the department. She has more than 40 publications to her credit in reputed international journals and international conferences. She can be contacted at email: ashapalal@gmail.com.